BL1A

Oscillator Strength Sum Rule of Sulfur K-edge NEXAFS Spectra of Sulfur-Containing Amino Acids

Y. Izumi, M. Tanabe, K. Sugiki and K. Nakagawa
Graduate School of Human Development and Environment, Kobe University, Kobe 657-8501, Japan

Absolute values of optical absorption cross section $\sigma(h\nu)$ as a function of photon energy $h\nu$ over the wide range, is a fundamental and important data for molecular science. Synchrotron radiation is very powerful as a continuum light source to measure $\sigma(h\nu)$ within the wide energy range. Here we report our experimental result to measure the $\sigma(h\nu)$ spectra with the focus at the near edge X-ray absorption fine structure NEXAFS for the sulfur K-edge region.

The reason why we measured the sulfur K-edge NEXAFS spectra is that sulfur is the heaviest atom within amino acid molecules [1, 2] which have been found in many meteorites and thus are believed to be formed in space in prior to the emergence of the first life. Our objective to measure the sulfur K-edge NEXAFS spectra is to study the role of sulfur atoms in the chemical evolution.

Methionine (Met) and cystin (Cys) were purchased from Wako Chemical company. Putting amino acid powder between 7.5 um polyimide films, we pressed and prepared pellet samples of which thickness were about 5 to 30 μm. NEXAFS spectra measurement were carried out at the beamline 1A by the transmittance mode with the double crystal monochromator equipped with InSb crystals. Analyzing the transmitted X-ray intensities I_0 $(h\nu)$ for polyimide films and $I(h\nu)$ for the amino acids and polyimide, we determined relative values of absorption cross section. Assuming that absolute values of cross section around 2460 eV and 2560 eV should be equal to the sum of atomic absorption cross sections [3] of each constituent atom making the amino acid molecule, we determine the absolute values of $\sigma(h\nu)$. Obtained results are shown in Fig. 1.

After detailed analyses of the NEXAFS spectra shown in Fig. 1 using the DV-Xα calculation, we found that our spectra could not resolve the chemical shift components of S-S bond and S-C bond, probably due to relatively worth resolution energy ($\Delta h\nu$ = 1.5 eV) of the measurement system with the InSb crystals. More detailed spectra with the higher resolution energy ($\Delta h\nu$ = 0.5 eV) were reported by Risberg et al.[2] with the Si crystals.

In spite of the worth resolution energy, we examined our spectra in terms of the oscillator strength sum rule in which integrated oscillator strength n_o should be equal to the number n_e of electrons responsible to the optical transition within the subjected energy region. By the integration of $\sigma(h\nu)$ from 2460 eV to 2590 eV, we obtained n_o to be 0.25 for Cyt. This value is reasonable to the report by Reynaud et al. [4] for H_2S, SO_2 and SF_6, n_o values of which molecules are 0.13, because n_o = 4 of Cyt is twice of n_o = 2 of H_2S, SO_2 and SF_6. The integration of $\sigma(h\nu)$ from 2460 eV to 2800 eV gave 0.3 for Met. This value was also reasonable with comparison to 0.31 for H_2S, SO_2, and SF_6 reported by Reynaud et al. [4].

We concluded that sulfur atom plays an important role in chemical evolution in space because x-ray photons can be absorbed with higher efficiency by the sulfur containing amino acids than those without sulfur atoms. This effect may be compared to the effect of antenna to absorb the electromagnetic waves with higher efficiency.

This work was done by the joint study program of UVSOR 20-804 and 21-506.

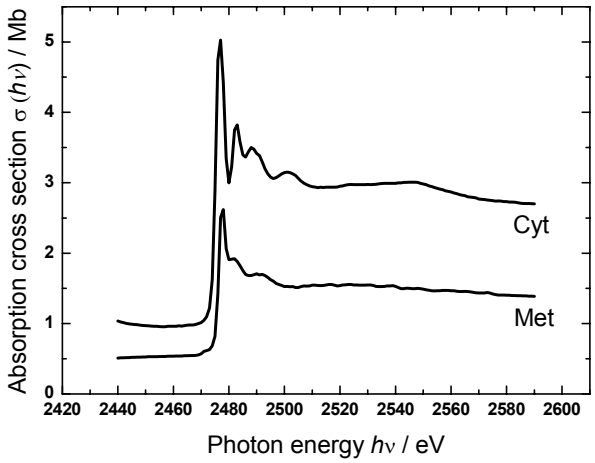

Fig. 1. Absolute values of absorption cross sections of cystin (Cyt) nad Methionine (Met).

[1] J. Siritapetawee and W. Pattanasiriwisawa, J. Synshrotron Rad. **15** (2008) 158-161.
[2] E. D. Risberg *et al.,* The Royal Society of Chemistry 2009 Dalton Trans. (2009) 3542-3558.
[3] B. L. Henke *et al.,* Atomic Data and Nuclear Data Tables **54-2** (1993) 181-342.
[4] C. Reynaud *et al.,* J. Phys. B: At Mol. Opt. Phys. **29** (1996) 5403-5419.

BL2B

Exclusive Detection of Photofragments from C_{60} with a Potential-Switch Mass Selector

H. Katayanagi[1, 2], Md. S. I. Prodhan[1], B. P. Kafle[1], C. Huang[1] and K. Mitsuke[1, 2]
[1]*Dept. of Photo-Molecular Science, Institute for Molecular Science, Okazaki 444-8585, Japan*
[2]*Graduate University for Advanced Studies (SOKENDAI), Okazaki 444-8585, Japan*

We have developed a potential-switch mass selector (PMS) incorporated into the apparatus of velocity map imaging for the photofragmentation of fullerenes. The performance of the PMS was tested by time-of-flight (TOF) mass spectrometry of the photofragments from C_{60}. A peak of C_{54}^{2+} was exclusively detected with a sufficient mass resolution.

The structure of our photofragment mass spectrometer used in the present experiment is almost identical to that described elsewhere [1, 2]. The fullerene (C_{60}) sample was loaded in a cylindrical quartz cell and heated up to around 700-800 K in vacuum. The C_{60} vapor sublimated from the cell passed through two apertures and reached the ionization region, and irradiated with the monochromatized synchrotron radiation. Ions produced at the ionization region were extracted by a Wiley-McLaren type electrode assembly, which consists of the ion repeller, extractor and entrance plate of an ion drift tube. The ions were pushed out by a pulse voltage (75 V, 4.5 μs, 1.1 kHz) applied to the repeller and projected on to a Z-stack MCP of 27 mm in diameter. The MCP was located 375 mm away from the ionization region. The ion drift tube was kept at -340 V and the extractor at 1 V.

The PMS is composed of a mass gate and an ion reflector. They were installed in the end of the ion drift tube. Their dimensions and positions were optimized by ion trajectory simulation [1, 3]. Thin meshes were attached to the both ends of the mass gate in order to avoid the distortion of the equipotential surfaces due to a fringe effect. The ion reflector consists of a triplet of disk electrodes that have central holes covered with fine meshes. The second disk electrode named "retarding grid" was placed 5 mm apart from the first and third disk electrodes that were kept at -340 V. These two electrodes made the equipotential surfaces flat and parallel inside the ion reflector.

The retarding grid was biased to 80 V. Eventually all the ions were forced back there and cannot enter the MCP. We then applied a pulse voltage changing from -340 to V_G = 100 V to the mass gate by a home made pulse generator. Instantaneously the potential energies of the ions were elevated the ions of interest were made to pass through the retarding grid and reach the MCP, if we had adjusted the application timing of V_G to their arrival time into the mass gate. For the control experiment we applied DC voltages of -340 and 0 V to the mass gate and retarding grid, respectively. This combination resulted in no mass discrimination and allowed all the ions to go beyond the ion reflector.

Figure 1(a) shows TOF mass spectrum of the photofragments in the control experiment. All the parent and fragment ions reached the detector. The presence of PMS has no essential effect on the mass resolution. Figure 1(b) shows the TOF spectrum of doubly charged ions which were selected with PMS. A pulse voltage applied to the mass gate was at 24 μs after the repeller pulse and 3 μs in width. The parent and fragment ions were selected without any distortion. With applying the shorter pulse voltage of 0.7 μs, we succeeded in selecting the C_{54}^{2+} peak without any distortion and contamination from neighboring peaks. The selected C_{54}^{2+} peak is shown in Fig. 1(c).

From the present result we can expect that the mass selective imaging experiment can be conducted using the PMS with replacement of the MCP by a position sensitive detector.

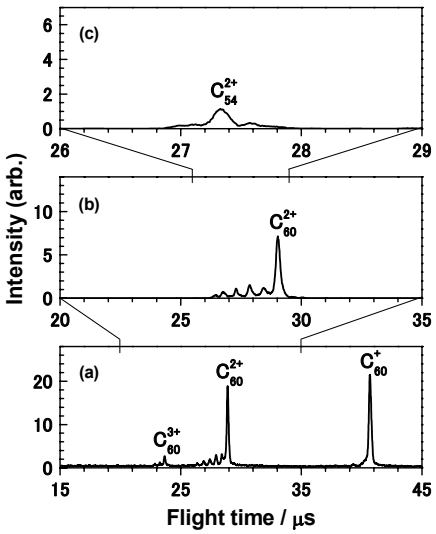

Fig. 1. TOF spectra of C_{60} at $h\nu$ = 90 eV. (a) The control experiment; (b) and (c) the discrimination of all species in doubly charged states and C_{54}^{2+}, respectively.

[1] H. Katayanagi *et al.*, in the proceedings of Pure and Applied Chemistry International Conference 2010 (PACCON2010), Thailand, PTC-P0-45.
[2] Md. S. I. Prodhan *et al.*, Chem. Phys. Lett. **469** (2009) 19.
[3] B. P. Kafle, H. Katayanagi and K. Mitsuke, AIP Conf. Proc. **879** (2007) 1809.

BL2B

Development of a TEPICO Technique for Determination of Excess Energy Partitioning in Dissociative Photoionization

H. Katayanagi[1, 2], Md. S. I. Prodhan[1], B. P. Kafle[1], C. Huang[1] and K. Mitsuke[1, 2]

[1]*Dept. of Photo-Molecular Science, Institute for Molecular Science, Okazaki 444-8585, Japan*

[2]*Graduate University for Advanced Studies (SOKENDAI), Okazaki 444-8585, Japan*

We have observed ion yield spectra of photofragments produced by the dissociative photoionization of fullerenes. Maximum internal energies of parent ions were estimated from appearance photon energies of the fragments. The obtained maximum internal energies agreed well with those calculated on the basis of the RRKM theory [1]. So far in our discussion kinetic energies of photoelectrons were assumed to be zero. In order to remove this crude assumption a coincidence technique was developed. In this technique photofragments are detected in coincidence only with the electrons with zero-kinetic-energy or threshold photoelectrons.

In the beginning we observed the threshold ion yield spectra of He at the first ionization energy by means of the threshold photoelectron photoion coincidence technique (TEPICO) developed in the present study. We then evaluated the feasibility of this technique to experimentally elucidate the photodissociation mechanism of fullerenes.

The helium gas was introduced to a vacuum chamber through a 1/4' tube. Helium atoms were ionized with the monochromatized synchrotron radiation at an ionization region between an ion repeller (R) and ion extractor (E) electrodes. The electrode R also acts as the entrance to an electron detector. The photoelectrons were detected by a chevron MCP. In order to select the threshold electrons we made use of the "dark gaps" in the temporal profile of a bunch structure of UVSOR. There is a 20-40 ns dark gap in every 176 ns. No ionization takes place during the dark gap. While the threshold electrons remain at the ionization region during the dark gap, high-energy electrons escape immediately. Only the threshold electron signals were detected by application of a pulse voltage (-3 V, 30 ns) to the electrode E at the timing of the dark gap. This synchronization of the pulse voltage with the dark gap was achieved with a "pick-up" signal (5.68 MHz) supplied from the UVSOR. The pick-up signal was frequency-divided by 8-10 in order to fit it to the maximum triggering rate of the apparatus.

Electron TOF spectra were measured with respect to the pick-up signal. A peak of threshold electrons was observed. The threshold electron signal was used to trigger a pulse voltage (75 V, 4.5 μs) applied to the electrode R. The ions produced simultaneously with threshold electrons are thus extracted and projected on to a Z-stack MCP.

Figure 1 shows threshold photoelectron spectra of He. A peak was clearly observed at 24.6 eV which agreed well with the first ionization potential of He. The resolution was found to be *ca.* 50 meV from the full-width at half-maximum of the peak. An ion yield curve of He obtained by the TEPICO method is shown in Fig. 2. A peak of 20 meV in width was clearly observed at 24.6 eV.

We succeeded in obtaining the TEPICO spectra of He. The present resolution of 20 meV was found to be sufficient to discuss the energy-partitioning mechanism on a basis of the transient-state theory. However, we have not yet succeeded in obtaining TEPICO spectra of other samples than He. This is due to low collection efficiency of the threshold electron in the present method since the electrons are collected only when the pulse voltage is applied during the dark gap. It is insufficient to discriminate small number of threshold electrons from large amount of energetic electrons. This is the case with most of samples except He. We will fabricate the electron detector that has a higher efficiency to collect threshold electrons.

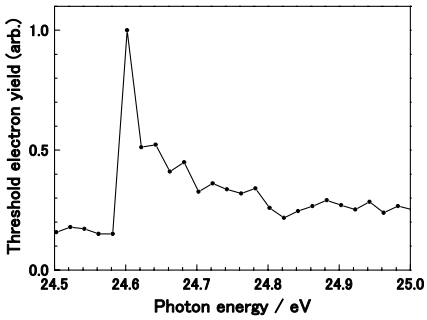

Fig. 1. Threshold photoelectron spectrum of He.

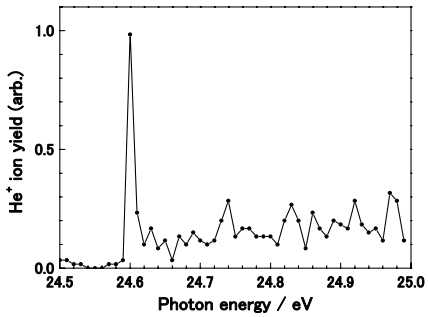

Fig. 2. Ion yield curve of He obtained by TEPICO.

[1] J. Kou *et al.*, Phys. Chem. Chem. Phys. **7** (2005) 119.

BL3U

Small Kr-Xe Mixed Clusters Studied by X-Ray Photoelectron Spectroscopy

M. Nagasaka[1], N. Kosugi[1] and E. Rühl[2]

[1]*Institute for Molecular Science, Myodaiji, Okazaki 444-8585, Japan*

[2]*Physikalische Chemie, Freie Universität Berlin, Takustr. 3, D-14195 Berlin, Germany*

Heterogeneous clusters mixed with different atoms show richer behavior than single atomic clusters. The structures of small mixed clusters have been investigated by theoretical simulations such as Monte Carlo method [1], and these results suggest that the structures are dependent on competition of several factors, such as atomic radii, surface energies, and interaction energies between different atoms. But there exist few experiments to study the structures of small mixed clusters. Recently, we have measured X-ray photoelectron spectroscopy (XPS) of the Kr_{30} clusters, and observed different binding energy shifts dependent on the surface site [2]. These shifts are derived from the induced polarization of surrounding atoms on the photoionization, and reflect the local environments. In this work, we have studied the structure of small Kr-Xe mixed clusters with different compositions by using XPS.

The experiments were performed at BL3U. The Kr-Xe mixed clusters were formed by the supersonic expansion of the primary gas mixtures with the Xe 1 – 5 % regions. The average compositions of the mixed clusters were estimated to be the Xe_5Kr_{27}, $Xe_{11}Kr_{26}$, $Xe_{15}Kr_{22}$, and $Xe_{22}Kr_{14}$ at the 1, 2, 3, and 5 % Xe conditions, respectively.

Figure 1 shows the Xe $4d_{5/2}$ XPS spectra at different compositions. All the sites in the Xe_5Kr_{27} clusters show smaller binding energy shifts than those in the Xe_{30} clusters. Because the polarizability of Kr is smaller than that of Xe, the smaller shifts mean that the Xe atoms contact with the Kr atoms. The peak intensities of bulk sites are close to those of edge sites in the Xe_5Kr_{27} clusters. These results suggest that the small Xe_5 core is embedded on the surface of the Kr clusters in the Xe_5Kr_{27} clusters.

In the $Xe_{11}Kr_{26}$ clusters, the edge and bulk sites are slightly shifted to the lower binding energies from the Xe_5Kr_{27} clusters. By calculating the binding energy shifts considering the induced polarization, we found that the two Xe cores exist on the surface of the Kr clusters. The single component cluster below the size of 200 shows icosahedron structures, where the surface is not closed packed structures [3]. The space in the Kr surface is filled by the Xe cores, and the Kr clusters show the denser structures. As a result, the Xe cores move to the outer parts of the Kr clusters, and the peak intensities of the edge sites are increased compared to those of the bulk sites. In the $Xe_{15}Kr_{22}$ clusters, the Xe cores are growing up on the surface of the Kr clusters and merged with each other because the Kr clusters have no space for the formation of the additional Xe cores.

In the $Xe_{22}Kr_{14}$ clusters, the binding energies of the edge and bulk sites are shifted to the lower binding energy. These results indicate that the separated layer between the large Xe and Kr clusters are formed in the $Xe_{22}Kr_{14}$ clusters.

In conclusion, we have revealed the structures of the small Kr-Xe mixed clusters, in which the structures are changed dynamically with the different mixing ratios. We also confirmed that these structures are consistent with the theoretical results [1].

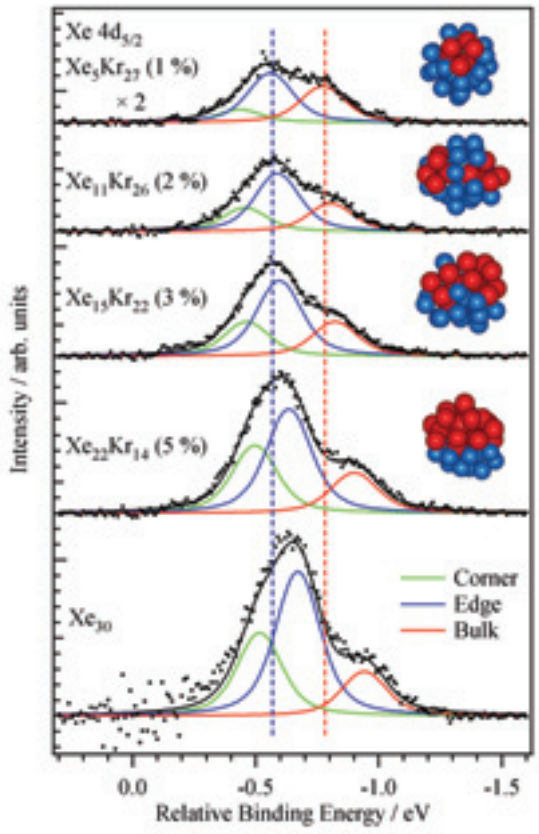

Fig. 1. The Xe $4d_{5/2}$ XPS spectra for the mixed clusters with different compositions, where the average size is shown. The atomic signal was subtracted, and the binding energy of the Xe atom was set to be zero. The proposed models are also shown, in which the blue and red spheres represent the Kr and Xe atoms, respectively. The sizes of the model structures are set to be 35.

[1] F. Calvo and E. Yurtsever, Phys. Rev. B **70** (2004) 045423.

[2] T. Hatsui *et al.*, J. Chem. Phys. **123** (2005) 154304.

[3] S. Kakar *et al.*, Phys. Rev. Lett. **78** (1997) 1675.

BL3U

Development of Liquid Cell with Different Thickness for Soft X-Ray Absorption Spectroscopy of Aqueous Solutions in Transmission Mode

M. Nagasaka[1], T. Hatsui[2], T. Horigome[1] and N. Kosugi[1]
[1]*Institute for Molecular Science, Myodaiji, Okazaki 444-8585, Japan*
[2]*XFEL Project Head Office, RIKEN, Sayo-cho, Hyogo 679-5148, Japan*

X-ray absorption spectroscopy (XAS) is a powerful method to investigate local electronic and geometric structures around core-excited atoms. But the chemically important inner shells such as C, N, and O K-edges are difficult to apply XAS in transmission mode because of the short attenuation length of soft X-rays. XAS is mainly applied in the vacuum condition by collecting secondary ions, electrons, and fluorescence following the inner-shell excitations. Recently, O K-edge XAS spectra of liquid water were measured with the yields of the secondary processes [1]. There exist several debates in the interpretation of the liquid water. In order to settle the discussion, the transmission measurement is very important. Näslund *et al*. successfully measured XAS in transmission mode [2]. In the present study, we have developed a thickness controllable liquid cell for the O K-edge XAS of aqueous solutions in transmission mode [3].

Figure 1(a) shows a diagram of our liquid flow cell. There are four regions I, II, III, and IV, separated by 100 nm-thick SiN_x membranes (NTT-AT N Co.). The region I is connected to BL3U in a vacuum condition. The regions II and IV are in an atmospheric condition of helium gas, where the pressure is controllable. The pressure difference between the regions I and II is quite large. The SiN_x membranes with the sizes of 200 × 200 μm^2 are settled in this border. Soft X-rays in the region I pass through the region II and the liquid layer in the region III, and reach a photodiode detector in the region IV. In order to transmit soft X-rays at the O K-edges, the thickness of the liquid layer should be below 1 μm. The gap in the region III is formed by sandwiching two SiN_x membranes with the sizes of 2 × 2 mm^2. As shown in Fig. 1(b), the two 20 μm-thick Teflon sheets are put as a spacer and pressed with the sealed O-rings. The fresh liquid is supplied with a tubing pump system during changing the photon energy, and suspended automatically at the absorption measurement of the destination photon energy. The XAS spectrum was obtained as $\ln(I_0/I)$, in which the currents I_0 for the blank cell and I for the sample cell. The contributions of the high order X-rays were removed in this spectrum.

Figure 2 shows the transmission O K-edge XAS for liquid water at room temperature by changing the He backpressure (0 to 10 kPa) in the regions II and IV. As a result, the thickness is ranged from 700 nm to 200 nm. The three characteristic features are obtained as the pre-edge peak (~535.5 eV), the main-edge (~537 eV), and the post-edge maximum (~540 eV). The ratio of pre-edge to main-edge becomes 0.49. These results are consistent with the previous transmission results (0.4) [2].

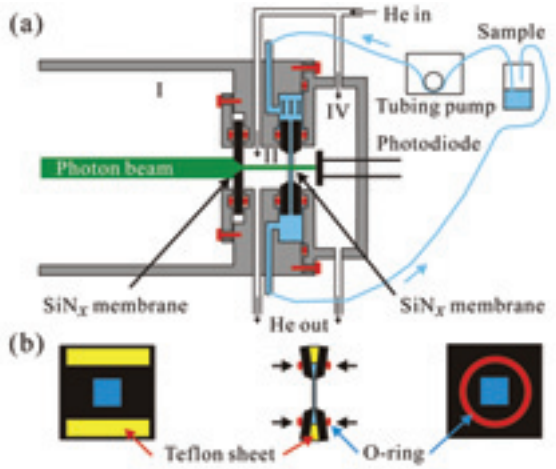

Fig. 1. (a) A schematic liquid flow cell for the soft X-ray transmission measurements. (b) The details of the thin liquid layer in the region III.

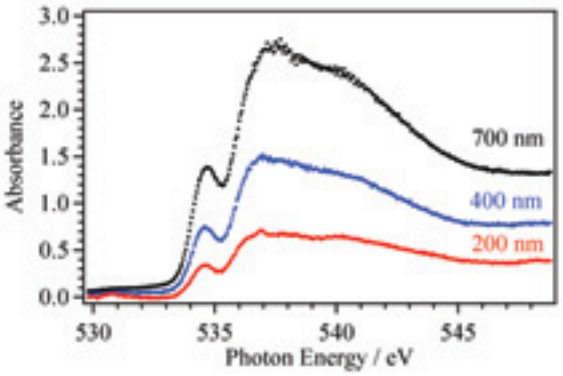

Fig. 2. O K-edge X-ray absorption spectrum of the liquid water with the thickness from 700 nm to 200 nm by controlling the He backpressures.

[1] Ph. Wernet *et al*., Science **304** (2004) 995.
[2] L.-Å. Näslund *et al.*, J. Phys. Chem. B **109** (2005) 13835.
[3] M. Nagasaka *et al*., J. Electron Spectrosc. Relat. Phenom. **177** (2010) 130.

BL6U

Doppler Effect in Fragment Autoionization Following Core-to-Valence Excitation of O_2

R. Guillemin[1], M. Simon[1] and E. Shigemasa[2]

[1]*LCPMR, Université Pierre et Marie Curie, 75231 Paris Cedex 05, France*

[2]*UVSOR Facility, Institute for Molecular Science, Okazaki 444-8585, Japan*

The Doppler effect is known to occur when the source and observer are in motion relative to each other, leading to an apparent change in the observed frequency of the propagating wave. This effect has a wide variety of applications in many fields, relating to the sensing of movement. In the research field of molecular physics, the sensing of nuclear motion has long been an important issue. Gel´mukhanov and co-workers predicted in 1997 [1] that the nuclear motion in 'ultrafast dissociation' following molecular core-level photoexcitation can be probed by the Doppler effect in emitted Auger electron. Ultrafast dissociation is a process in which the molecular dissociation at the core-excited state precedes the Auger decay and then an atomic fragment emits an Auger electron [2]. The atomic Auger electron can possess the opposite Doppler shift depending on the direction approaching the detector or moving away from it.

The electronic Doppler effect on ultrafast dissociation was experimentally evidenced for the first time at the core-to-valence excitation in O_2 [3]. Recently, the electronic Doppler effect after the core-to-Rydberg excitations in N_2 has been revealed [4]. In the present work, similar experiments for observing slow electron emissions from atomic fragments have been conducted for the core-to-valence excitation of O_2.

The experiment was performed on the soft X-ray beamline BL6U at UVSOR. The radiation from an undulator was monochromatized by a variable included angle varied line-spacing plane grazing monochromator. The photon energy resolution E/ΔE was set to 2000. The monochromatized radiation was introduced into a cell with sample gases. Kinetic energies of the emitted electrons were measured by a hemispherical electron energy analyzer (MBS-A1) placed at a right angle with respect to the photon beam direction. The degree of the linear polarization of the incident light was essentially 100%, and the direction of the electric vector was set to be parallel to the axis of the electrostatic lens of the analyzer. The kinetic energy resolution of the analyzer was set to 25 meV for autoionizing slow electrons, and 60 meV for atomic Auger electrons.

Figure 1 shows the blowup of the atomic Auger line following the ultrafast dissociation [3] in the resonant Auger spectrum obtained at 539.43 eV, where the lower σ* resonance without overlapping with any Rydberg state lies. The atomic Auger line clearly demonstrates the Doppler splitting. Figure 2 displays an autoionizing slow electron spectrum measured at the same photon energy. All the peaks observed are assignable to the autoionization of O* into O^+, which exhibit double peak structures due to the Doppler effect. The kinetic energy releases estimated from the Doppler splittings seen in Fig. 1 and 2 are nearly the same. This means that the ultrafast dissociation following the σ* excitation produces two excited oxygen atoms: one is core excited and the other excited in the valence shell. The detailed data analysis is now in progress.

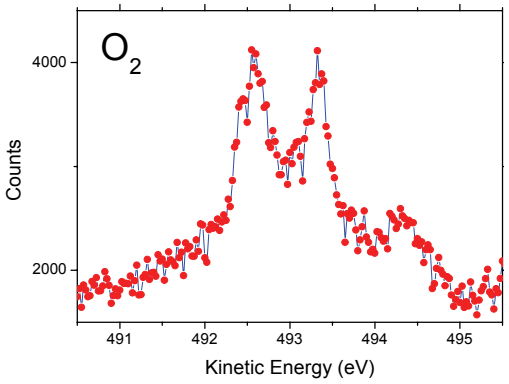

Fig. 1. Doppler profile of atomic Auger line measured at the lower σ* resonance position of O_2.

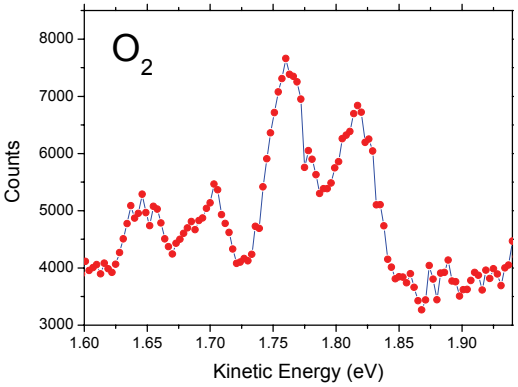

Fig. 2. Doppler profile of atomic autoionization line measured at the lower σ* resonance position of O_2.

[1] F. Gel´mukhanov, H. Ågren and P. Sałek, Phys. Rev. A **57** (1998) 2511.

[2] P. Morin and I. Nenner, Phys. Rev. Lett. **56** (1986) 1913.

[3] O. Björneholm *et al.,* Phys. Rev. Lett. **84** (2000) 2826.

[4] E. Shigemasa *et al.,* submitted to New J. Phys.

BL6U

High Resolution Electron Spectroscopic Study on Cascade Double Auger Processes After Ar 2p Photoionization

P. Lablanquie[1] and E. Shigemasa[2]

[1]*LCPMR, Université Pierre et Marie Curie, 75231 Paris Cedex 05, France*

[2]*UVSOR Facility, Institute for Molecular Science, Okazaki 444-8585, Japan*

An inner shell vacancy created by photoionization decays either via emission of radiation (fluorescence) or electron emission (Auger decay). The Auger decay is generally more favorable for L-shells, which can occur with emission of one electron (single Auger decay) or of a few electron (multiple Auger decay). The probability of multiple Auger decay is usually lower than that of single Auger decay, but can be high enough to allow experimental observations. Thanks to the recent progress in coincidence measurements, the path toward a deeper understanding of double Auger (DA) decays, where the filling of the inner shell vacancy by an outer electron causes the ejection of two electrons, has been opened [1]. This process can be divided into two categories: the direct double Auger decay (DDA) when the two electrons are emitted simultaneously, and cascade double Auger decay (CDA) when the electron emission occurs in two sequential steps.

More recently, coincidence measurements based on the utilization of magnetic bottle time of flight electron spectrometers have opened the possibility to obtain the complete state selected triple photoionization (TPI) continua over a wide range of kinetic energies [2]. The application of this method to the multi-electron decays of the Ar 2p shell [3] reveals that the position and shapes of the photoelectron lines related to the DA decay differ for the DDA and CDA processes [4]. Moreover, the peak profiles assigned to the DA processes are strongly distorted by post collision interaction (PCI) effects [4]. Post-collision interaction (PCI) is an exchange of energy between charged particles, usually electrons, emitted in single events. PCI in single Auger decay following inner shell photoionization is well investigated both experimentally and theoretically. However, PCI in the DA processes has been much less studied so far.

In order to obtain the detailed spectroscopic information on the Ar^{2+} states involved in the CDA decay, high resolution electron spectroscopy has been applied to the study of the decay processes following the 2p photoionization of Ar. High resolution electron spectra were obtained on BL6U at UVSOR, by using a high performance hemispherical electron energy analyzer MBS-A1, developed by the MB Scientific AB company. The experimental setup is equipped with a gas cell, and reaches a theoretical 1.3 meV (FWHM) resolution when operated with a pass energy of 2 eV and a slit opening of 0.2 mm.

As an example, a high resolution electron spectrum for the strongest second-step Auger electron in the following CDA process is shown in Fig. 1:

$$Ar + h\nu \rightarrow e_1 + Ar^{+}*(2p^{-1}{}_{1/2,3/2})$$
$$\rightarrow e_1 + e_{1A}(E_2) + Ar^{2+}*$$
$$\rightarrow e_1 + e_{1A}(E_2) + e_{2A}(E_3) + Ar^{3+}((3p^{-3})\ {}^4S, {}^2D, {}^2P).$$

The spectrum of Fig. 1 was measured at the photon energy of 270 eV, in order to minimize the PCI distortion of the peaks. During the course of the experiments, slow drift of the peak positions occurred with time, which was minimized by short scans of less than a few minutes. The main peak at 2.19 eV corresponds to the second Auger electron emitted in the CDA path, associated with the Ar^{2+}* state of 86.31 eV (A1) binding energy, which decays towards the $Ar^{3+}(3p^{-3}\ {}^4S)$ final state [3]. The shoulder on the high energy side of the peak is attributed to the contribution of a weak CDA path mediated by an Ar^{2+} intermediate state different from A1. Through the analysis of the peak width in a series of similar measurements, it is found that a lifetime broadening of the corresponding intermediate state is 3.7 ± 0.4 meV, taking into account the theoretical resolution of 1.3 meV for the analyzer and the Doppler contribution of 2.9 meV.

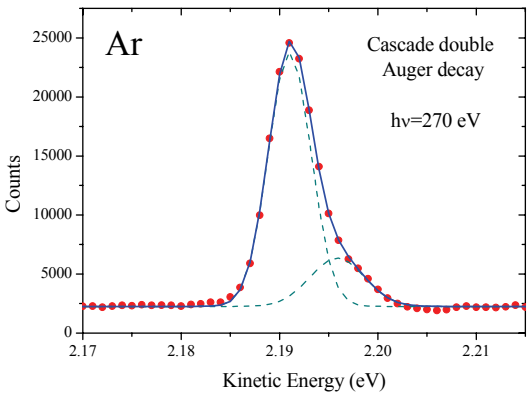

Fig. 1. Cascade double Auger electron spectrum measured with the MBS-A1 analyzer at the photon energy of 270 eV.

[1] F. Penent *et al.,* Phys. Rev. Lett. **95** (2005) 083002.

[2] Y. Hikosaka *et al.,* Phys. Rev. Lett. **102** (2009) 013002.

[3] P. Lablanquie *et al.,* J. Electron Spcetrocs. Relat. Phenom. **156-158** (2007) 51.

[4] S. A. Sheinerman *et al.,* submitted to J. Phys. B.